Ventral tegmental area dopamine neural activity switches simultaneously with rule representations in the prefrontal cortex and hippocampus

Abbreviated title: Dopamine-CA1-PFC activity during rule switching

Authors: Mingxin Ding[1], Porter L. Tomsick[2,3], Ryan A. Young[4], Shantanu P. Jadhav[1,4,5]

[1]Graduate Program in Neuroscience, Brandeis University, Waltham, MA 02453, USA

[2]Undergraduate Program in Neuroscience, Brandeis University, Waltham, MA 02453, USA

[3]Department of Neuroscience, Virginia Polytechnic Institute and State University, Blacksburg, VA 24061, USA

[4]Department of Psychology, Brandeis University, Waltham, MA, 02453, USA

[5]Volen National Center for Complex Systems, Brandeis University, Waltham, MA, 02453, USA

Contributions: M.D. and S.P.J. conceptualized the study; M.D. and P.L.T. performed the experiments; M.D. analyzed the data; R.A.Y. contributed to analysis packages; M.D. and S.P.J. wrote the manuscript.

Correspondence: Shantanu P. Jadhav (shantanu@brandeis.edu), Brandeis University, 415 South St., MS 062, Waltham, MA 02453

Number of Pages: 42

Number of Figures: 5 figures

Number of Tables: 1 table

Number of words: Abstract (249 words); Significance statement (119 words); Introduction (657 words); Discussion (1431 words)

Acknowledgements: This work was supported by the National Institutes of Health (R01MH112661) to S.P.J. and a T90 training grant (R90DA033463). We would like to thank Dr. Naoshige Uchida, Dr. Joshua Berke and Dr. Ali Mohebi for the protocol of the opto-tagging experiment, Dr. John Bladon and Audrey Hooker for piloting the W-track rule switching task, Dr. Justin Shin in assisting in implant surgeries, Dr. Wenbo Tang, Dr. Jacob Olson, Dr. Blake Porter and other lab members in providing feedback on the research project.

Conflicts of Interest: Authors report no conflict of interest.

Abstract

Multiple brain regions need to coordinate activity to support cognitive flexibility and behavioral adaptation. Neural activity in both the hippocampus (HPC) and prefrontal cortex (PFC) is known to represent spatial context and is sensitive to reward and rule alterations. Midbrain dopamine (DA) activity is key in reward seeking behavior and learning. There is abundant evidence that midbrain DA modulates HPC and PFC activity. However, it remains underexplored how these networks engage dynamically and coordinate temporally when animals must adjust their behavior according to changing reward contingencies. In particular, is there any relationship between DA reward prediction change during rule switching, and rule representation changes in PFC and CA1? We addressed these questions using simultaneous recording of neuronal population activity from the hippocampal area CA1, PFC and ventral tegmental area (VTA) in male TH-Cre rats performing two spatial working memory tasks with frequent rule switches in blocks of trials. CA1 and PFC ensembles showed rule-specific activity both during maze running and at reward locations, with PFC rule coding more consistent across animals compared to CA1. Optogenetically tagged VTA DA neuron firing activity responded to and predicted reward outcome. We found that the correct prediction in DA emerged gradually over trials after rule-switching in coordination with transitions in PFC and CA1 ensemble representations of the current rule after a rule switch, followed by behavioral adaptation to the correct rule sequence. Therefore, our study demonstrates a crucial temporal coordination between the rule representation in PFC/CA1, the dopamine reward signal and behavioral strategy.

Significance Statement

This study examines neural activity in mammalian brain networks that support the ability to respond flexibly to changing contexts. We use a rule-switching spatial task to examine whether the key reward-responsive and predictive dopamine (DA) activity changes in coordination with changes in rule representations in key cognitive regions, the prefrontal cortex (PFC) and hippocampus. We first established distinct rule representations in PFC and hippocampus, and predictive coding of reward outcomes by DA neuronal activity. We show that the rule-specific DA reward prediction after a rule switch develops in temporal coordination with changes in rule representations in PFC, eventually leading to behavioral changes. These results thus provide an integrated understanding of reward prediction, cognitive representations of rules and behavioral adaptation.

Introduction

Behavioral flexibility is critical to survival and for adapting to a changing environment. These functions are frequently driven by changing reward conditions and supported by distributed network processing in the brain to evaluate context and respond appropriately. The hippocampal cognitive map represents spatial context (O'Keefe and Dostrovsky, 1971; O'Keefe, 1978), and hippocampal neuronal activity can also be modulated by rewards and goals (Lee et al., 2012; Gauthier and Tank, 2018; Krishnan et al., 2022). The prefrontal cortex (PFC) serves complementary cognitive functions including working memory, executive control, and context representation (Ragozzino and Kesner, 1998; Yoon et al., 2008; Horst and Laubach, 2009; Durstewitz et al., 2010; Hyman et al., 2012; Urban et al., 2014; Ma et al., 2016). The hippocampus and prefrontal cortex have been demonstrated to coordinate temporally for adaptation of behavioral strategy when experiencing environmental/contextual changes (Guise and Shapiro, 2017; Hasz and Redish, 2020). However, much remains unexplored about how reward signals, acting as major feedback to animals' state/action choices, coordinate with this navigation and memory system for cognitive flexibility and behavioral adaptation. The dopamine (DA) signal from the midbrain is known to be involved in reward prediction error processing (Schultz et al., 1993, 1997) and value estimates (Roesch et al., 2007; Howe et al., 2013; Hamid et al., 2015; Dabney et al., 2020), and is causally linked to learning (Steinberg et al., 2013; Hamid et al., 2015). DA release profile and firing activity has also been reported to ramp up during reward approach and scale positively with reward quantity and probability (Howe et al., 2013; Engelhard et al., 2019; Krausz et al., 2023). How this DA signal changes during rule switches to support behavioral flexibility at short time scales of a few tens of trials over which behavioral change is observed remains less explored.

In this study, we were interested in examining the dynamics of rule and context representations in the hippocampal (area CA1) and prefrontal regions during reward-guided behavioral adaptation in response to rule switching, and whether these dynamics are related to

ventral tegmental area (VTA) DA neuronal activity. The primary hypotheses we aimed to test are whether changes in reward-associated DA neuronal firing activity are temporally coordinated with changes in rule representations in these cognitive regions as animals adapt to changes in contingencies over a few trials due to rule switching, thus supporting a role in cognitive flexibility. The PFC receives input from and sends output to midbrain DA neurons (Carr and Sesack, 2000; Beier et al., 2015; Kabanova et al., 2015; Morales and Margolis, 2017), and PFC and DA are known to contribute to reinforcement learning in a complimentary manner, with prefrontal signals encoding predictive values and dopamine encoding prediction errors (Lak et al., 2020). In addition, DA projections to dorsal hippocampus have been reported (Gasbarri et al., 1994), and CA1 place fields have been shown to change stability based on reward conditions and DA input (Martig and Mizumori, 2011; McNamara et al., 2014; Krishnan et al., 2022). It remains unknown if and how DA signal changes coordinate with rule and context representation in the CA1 and/or PFC, and the time scale of such coordination if it exists.

To investigate these questions, we implemented a novel rule-switching spatial task for rats in a W/M maze and recorded activity simultaneously from CA1, PFC and VTA ensembles as animals performed this task. We found single cell and ensemble codes of underlying rules in both the CA1 and PFC regions. VTA reward signaling and predictive coding of reward outcomes during maze running for the two rules were confirmed. We found that this rule-specific predictive feature of DA spiking activity develops together with correct PFC and CA1 rule decoding a few trials after a rule switch, followed by a change of behavioral strategy within a few trials. Together, this work establishes that the dynamics of DA spiking activity and PFC and CA1 rule representation changes occur in a coordinated manner during a rule switching task.

Materials and Methods

Animals and experimental design

Four adult male TH-Cre rats (450-600 g, 3-7 months, RRID: RRRC_00659) (Witten et al., 2011) were used in the current study for behavior and physiology data. All procedures were conducted under the guidelines of the US National Institutes of Health and approved by the Institutional Animal Care and Use Committee at Brandeis University. Animals were bred in house, kept under a 12h/12h light/dark schedule, with ad libitum food and water access till at least 10 weeks old prior to behavioral training and experiments. After daily handling and habituation to a sleep box (30cm long, 30 cm wide, 50 cm tall), animals were moderately food deprived to 85-90% of their initial weight to motivate reward-seeking behavior on an elevated linear track. Once reaching the criterion of obtaining 60 condensed milk rewards in a 20-min session, animals were allowed free access to food for at least a week before surgery. During surgery, virus AAV5-EF1a-DIO-hChR2(E123T/T159C)-mCherry was injected into VTA and a custom multi-tetrode microdrive with optrodes was implanted into CA1, PFC and VTA (see **Surgical procedures**). Tetrodes and optrodes were gradually lowered into the target regions in the time span of 3-4 weeks to allow virus expression while animals recovered and retrained on the linear track. Recordings were performed during the process of learning and rule switching on the W track (see **Behavioral paradigm**).

Behavioral paradigm

Post-recovery animals learned to perform a rule switching task on the W track (80 cm long of each arm, 7 cm wide, see **Figure 1A**). The task consists of two rules with similar structure but different sequence assignments. The first rule is a standard W track alternation task: animals must travel to the center arm (home) to obtain a milk reward when they set out from a side arm (inbound trajectories), whereas they need to alternate between the left and right arms when they start from the center (outbound trajectories) (Jadhav et al., 2012, 2016; Maharjan et al., 2018; Shin et al., 2019). The second rule presents altered identities between the left and center arm.

144 Therefore, the left arm becomes the new home, and animals must alternate between the center
145 and right arms for outbound trajectories. Once animals learned both rules, they were subject to
146 rule switching in blocks if performance of the current rule reached 80% correct. Rule switching
147 happened without external cues, requiring the animals to use only reward feedback to deduce
148 the change and switch to the optimal strategy for the new rule. During a recording day, animals
149 ran 3-4 epochs of 20-25 min duration. The run epochs were interleaved by 20-40 min sleep
150 epochs. It typically took animals 6-12 running epochs to learn each rule, and an additional
151 training of at least 3-4 days before they could switch rapidly between rules (3-4 switches/rule
152 blocks per day).

153 **Surgical procedures**

154 Each rat received virus injection and microdrive implantation during the surgery. Microdrive
155 fabrication and implantation procedures were similar to previous reports (Jadhav et al., 2012,
156 2016; Tang et al., 2017; Shin et al., 2019). Anesthesia was induced by ketamine, xylazine and
157 atropine cocktail and maintained by 0.5% - 2% isoflurane. 500 nL of AAV5-EF1a-DIO-
158 hChR2(E123T/T159C)-mCherry was injected into VTA bilaterally (AP: -5.6 mm, ML: ±1.0 mm,
159 DV: -7.8mm). 24 tetrodes each targeting dorsal CA1 (AP: -3.6 to -4.0 mm, ML: ±2.2 mm, DV: -
160 2.5 mm) and PFC (AP: +3.0 mm, ML: ±0.9 mm, DV: -2.5 to -3.0 mm), and two optrodes
161 targeting VTA, with each optical fiber surrounded by 8 tetrodes, were encased in a microdrive,
162 and implanted against the surface (for CA1 and PFC) or 2 mm into the brain (for VTA). Animals
163 received post-operative analgesia and were monitored closely for at least a week before food
164 restriction and behavioral experiments.

165 **Data acquisition and processing**

166 Upon approaching target regions, CA1 was identified by the characteristic EEG features,
167 including sharp-wave ripples (SWRs) and theta modulation. PFC depth was targeted to anterior
168 cingulate cortex (ACC) and prelimbic (PrL) regions. VTA was identified by finding
169 optogenetically tagged cells (see **Cell type identification** below). Electrophysiological data was

170 recorded at 30 kHz using Trodes through a 256-channel headstage (SpikeGadgets, San
171 Francisco, CA). Digital input/output signals of nose pokes and reward delivery were
172 simultaneously recorded. Video recordings of animal behavior were captured at 30 fps with
173 sync'd timestamps to the neural recording. All tetrodes were grounded to a screw above
174 cerebellum. Tetrodes of each brain region were referenced using the group average. Spiking
175 data was bandpass filtered between 600 Hz and 6 kHz, and local field potential (LFP) data was
176 bandpass filtered between 0.5 Hz and 400 Hz and down sampled to 1.5 kHz. Animal's position
177 was tracked using the cameraModule (SpikeGadgets) to identify the red/green LEDs attached to
178 the headstage and verified by the researcher.
179 Spikes were clustered using MountainSort4 (Chung et al., 2017) and followed by manual
180 inspection and curation in MountainView. Clusters with isolation score >0.9, noise overlap <0.05
181 and peak signal-to-noise ratio > 2 were accepted and included in this study.

182 **Histology**

183 After recording, animals were put under anesthesia and recording sites were lesioned by
184 passing a current of 30 μA through the electrode tips. Animals were then perfused 1-2 days later
185 using 4% formaldehyde and the brains were kept in 4% formaldehyde and 30% sucrose solution
186 until being sliced into 50-μm sections. The VTA slices were immuno-stained for TH and imaged
187 to verify colocalization of virus expression and anti-TH antibody at optrode implantation sites.
188 The CA1 and PFC slices were stained with cresyl violet and imaged to verify tetrode locations.

189 **Cell type identification**

190 Putative DA neurons were identified using optogenetic tagging at least 3 weeks after surgery
191 to allow virus expression. In the first or last sleep epoch of each recording day, a 473-nm light
192 was delivered to the VTA as 5- or 10-ms pulse trains at 1, 4, 10, 20 and 40 Hz to identify TH+
193 cells expressing ChR2, similar to previous studies (Cohen et al., 2012; Mohebi et al., 2019; Kim
194 et al., 2020). The power of the laser was calibrated to lie within the range of 5-20 mW/mm^2 at
195 the tip of the fiber to avoid spike waveform distortion. The light-evoked spike latency was then

tested using Stimulus-Associated spike Latency Test (SALT, Kvitsiani et al., 2013). Units with p value <0.001 were classified as putative DA neurons.

CA1 and PFC cells were separated into putative pyramidal neurons and interneurons using k-means clustering with parameters including spike width, peak asymmetry and mean firing rate (Barthó et al., 2004; Sirota et al., 2008; Shin and Jadhav, 2024).

Data analysis

Linearization and normalization

Each trial was defined as the time starting from leaving the last reward well, running on the track and arriving at the current reward well, until the end of the stay at the current reward well. There are six trajectories in total defined across the two rules. Occupancy of positions of each trajectory was binned into 40 equally sized spatial bins (5-6 cm/bin) on the track during running, and then binned for 100-ms temporal bins at the reward wells. The occupancy was then smoothed by a 5-bin wide Gaussian kernel. The firing activity of each cell is binned and smoothed in the same fashion and firing rates are normalized by occupancy. For dimension reduction and population activity analyses, firing rates were z-scored for each cell across all task epochs.

Behavior analysis

Behavioral performance of each animal on each recording day was estimated using a previously described state space model (Smith et al., 2004; Kim and Frank, 2009). Average reward rate was summarized for rule 1 to 2 and rule 2 to 1, respectively. For analysis separating performance stages, quantile ranges were set individually for each recording day to have equal number of trials for each performance category (**Figure 3F, 4F**). Behavior strategy was estimated by generating the trajectory transition matrix in a 20-trial block with a 1-trial sliding window. The Pearson's correlation between each transition matrix and the optimal-strategy

transition matrix of each rule was computed to determine which rule the animals are currently following (**Figure 3D, 5D**).

Spatial information

Spatial information was calculated according to Skaggs et al., 1992 to estimate the amount of spatial content of each cell's spiking activity:

$$I = \int_x \lambda(x)\, log_2 \frac{\lambda(x)}{\lambda}\, p(x) dx$$

where *I* is the spatial information measure in bits/second, *x* is spatial location of the animal, *p(x)* is the probability of the animal residing at location *x*, *λ(x)* is the mean firing rate of the cell at location *x*, and *λ* is the occupancy-weighted overall mean firing rate of the cell.

Dimensionality reduction with Consistent EmBeddings of high-dimensional Recordings using Auxiliary variables (CEBRA)

We used a newly developed nonlinear dimensionality reduction method, CEBRA, to uncover consistent and interpretable latent space of neural spiking data conditioned by behavioral variables (Schneider et al., 2023). Rewarded trials with performance better than 60th percentile of the day were selected for training in CEBRA (**Figure 3B, C**). 20% of these trials with good performance and all trials with worse performance were left out for testing. The training trials were balanced for trajectory identities and rules. We used supervised CEBRA-Behavior models for both single- and multi-animal training. Training labels included spatial-temporal bin, trajectory and rule. Spiking data from each brain region was trained separately for individual animals. Parameters for CEBRA training were largely coherent with the example implementation using rat hippocampus data in (Schneider et al., 2023), except for higher batch size and larger number of iterations to improve model performance:

model_architecture='offset10-model',

time_offsets=10,

batch_size=2048,

learning_rate=5e-4,

temperature=1,

output_dimension=3,

max_iterations=12000,

distance='cosine',

conditional='time_delta',

num_hidden_units=64

The whole data set was then transformed into 3D embeddings using the trained models. To reveal common features across animals, we took advantage of the multi-animal training from CEBRA. This method allows different dimensions (numbers of cells recorded) from different sessions/animals as inputs and maintains the label space across models. Therefore, the resulting embeddings across animals are directly comparable. For multi-animal training, trial selection, model parameters and subsequent transforming process were held the same as in single-session model training.

Rule decoding

A k-nearest neighbor (kNN) decoder was trained using the 3D embeddings of training data and used to decode the underlying rule for the testing data. Decoding performance of each trial was calculated as the ratio of bins with correct rule assignment (**Figure 3D**). The decoding accuracy curve was then smoothed using a Gaussian kernel. After a rule switch, a change point was identified as the trial from which decoding probability of the current rule was consistently higher than 50%. This process is done for embeddings from each brain region. We categorized the behavioral performance into low, mid and high by splitting the estimated performance into 1/3 of the trials for each day, and reported the proportion of trials with correct rule decoding in **Figure 3F**. To better estimate the timing of rule representation transitions, we used 5-fold validation for training CEBRA models and decoding, resulting in 5 estimates for each animal and each brain region, reflected in **Figure 3E, H, I**.

DA neuron firing rate analyses

Reward responsiveness is defined as showing differences ($p<0.05$) of firing rates at 200ms – 1200ms after the first nose poke between rewarded and unrewarded trials using Wilcoxon rank sum test. For firing rate comparisons across conditions in **Figure 4C**, firing rates are compared using Wilcoxon signed rank test for each spatial/temporal bin and Bonferroni corrected for multi-comparison.

The influence of behavioral factors on each DA cell's single-trial firing rates was estimated using multiple linear regression.

$$\mathbf{y} = \mathbf{X}\boldsymbol{\beta} + \boldsymbol{\varepsilon}$$

$\mathbf{y}$ is the mean firing rate of each trial during either running or the first 3 seconds of the outcome period. $\mathbf{X}$ is the estimated behavioral factors for each trial, which included: reward, binary outcome, rewarded or unrewarded; reward rate, an estimate of mean reward rate using the last 5 trials' outcome; trajectory reward rate, an estimated reward rate of a certain trajectory, using outcomes of the last 5 times that the animal took the same trajectory. This process is repeated for all DA neurons (n=20), for both the running and reward outcome firing rates. The resulting significant coefficient values and the proportion of significant coefficients were summarized in **Figure 4H**.

Results

We recorded neuronal activity simultaneously from the dCA1, PFC (anterior cingulate cortex and prelimbic regions) and VTA in adult male Th-Cre rats (n=4) using tetrodes in PFC and HPC and optical fibers surrounded by tetrodes in VTA (**Figure 1E-G**, see **Materials and Methods**), while animals performed a non-cued spatial rule switching task (**Figure 1A**). Both rules in the switching task consist of two types of trajectories with different memory demands: inbound trajectories that are rewarding at the home location regardless of the animals' travel history; and outbound trajectories that only reward animals when they choose the different arm from last non-home visit, requiring working memory. For rule 1 (standard W/-M maze alternation task), the middle arm is the home location and animals alternate between left and right arms for outbound trajectories. For rule 2, the home location is switched to the left arm, and the middle and right arms become outbound destinations. Animals learned the two rules and were subsequently trained to switch between the two rules with solely the feedback of reward outcomes, and no external cues signaling the rule switch (**Figure 1B**). Animals were first trained on Rule 1 and subsequently on Rule 2. After 7-10 days of learning and training, animals could switch between the rules 3-4 times within a recording day. Rule switching was triggered manually during a session after a threshold performance (>80% correct) was achieved on the current rule. Upon unexpected trial outcomes, animals adapted their behavioral choices quickly to obtain more rewards, evident in decreasing numbers of perseverative errors over time (**Figure 1D**). It took 17 trials on average to reflect a Rule 2 to 1 switch in behavior, and 22 trials for Rule 1 to 2 (**Figure 1C**). The Rule 1 to 2 direction was typically more difficult for animals to achieve due to spatial asymmetry of rule 2. During each day of recording, animals ran the tasks in 3-4 20-30 min sessions, which were interleaved by 20-40 min sleep sessions. In the first or last sleep session, opto-tagging was performed to identify putative DA neurons in VTA (**Figure 1H**). An example raster during one trial is shown in **Figure 1I**. Position and speed plots show animal motion and immobility at the destination reward well, and raster plots show

316 corresponding patterns in the three regions. Note that CA1 and PFC firing activity spans the
317 spatial locations on the track. A total of 143 CA1 neurons, 128 PFC neurons and 53 VTA
318 neurons (20 TH+ neurons) from 4 animals, one recording day for each, were included in this
319 study (**Table 1**).

320 **Table 1: Clustered cell counts by brain region and cell type**

Animal	CA1 Pyr	CA1 Int	PFC Pyr	PFC Int	VTA DA	VTA non-DA
TH105	34	7	26	4	4	7
TH212	14	5	34	5	8	11
TH510	44	5	30	2	3	6
TH605	31	3	25	2	5	9
Total	123	20	115	13	20	33

321

322 **CA1 and PFC neurons show differentiated activity across rules**

323 CA1 and PFC neurons show spatially modulated firing activity (O'Keefe and Dostrovsky,
324 1971; O'Keefe, 1978; Hyman et al., 2010; Zielinski et al., 2019), and their features have also
325 been implicated in rule and context representations (Wood et al., 2000; Eschenko and
326 Mizumori, 2007; Griffin et al., 2007; Rich and Shapiro, 2009; Durstewitz et al., 2010;
327 Ferbinteanu et al., 2011; Karlsson et al., 2012; Powell and Redish, 2016; Guise and Shapiro,
328 2017; Hasz and Redish, 2020). We therefore first asked the question if the firing activity of CA1
329 and PFC neurons can reflect the current rule by showing rule-specific activity on trajectories. As
330 firing activity of VTA neurons showed much weaker spatial modulation (**Figure 2E**), we focused
331 only on CA1 and PFC for this analysis. Single-unit remapping was investigated using firing
332 activity on the two common trajectories that lead to reward for correct trials for both rules (*Left-*
333 *to-Center*: inbound for Rule 1 and outbound for Rule 2, and *Center-to-Left*: outbound for Rule 1

334 and inbound for Rule 2), as lack of reward is known to destabilize firing activity on mazes
335 (Krishnan et al., 2022). We found cells showing remapped activity across the two rules in both
336 CA1 and PFC regions (**Figure 2A**; rules are run in alternating blocks with two blocks for each
337 rule). Some cells show rate remapping (**Figure 2A**, first example on left, CA1 excitatory cell),
338 and some cells exhibited relocation of spatial firing to a different part of the track (CA1 and PFC
339 excitatory cell examples). Additionally, reward-associated firing after the same physical
340 trajectory but in different rule contexts also showed robust differences (examples with significant
341 differences in **Figure 2B**). These firing changes are not a result of recording drift over time, as
342 similar patterns were observed both earlier and later in the day, with interleaved rule blocks.
343 Further, trial-wise cell firing vectors also exhibited increases in correlation with stable-
344 performance firing vectors of the current rule as behavioral performance improved, and become
345 less similar (lower correlation) after the rule changed (**Figure 2C**). Overall, we found that 27.3%
346 of hippocampal CA1 cells and 25.8% of PFC cells show significantly differentiated activity during
347 running based on the current underlying rule, and 14.7% CA1 and 14.8% PFC neurons during
348 reward. There was no significant difference in the ratio of rule-modulated neurons across
349 regions (**Figure 2D**).

350 **CA1 and PFC ensemble representations distinguish the rules and show transitions**
351 **during rule switching**

352 We next investigated ensemble activity changes across rules in CA1 and PFC, and the
353 dynamics of these changes in relationship to behavior. Trial-by-trial population vector similarity
354 was computed and aligned to the first trial after rule switching, shown in the correlation plots in
355 **Figure 3A**. Similar to previous research findings (Hasz and Redish, 2020), the firing pattern of
356 both regions stabilized toward the end of running one rule (seen as increase in correlation with
357 neighboring trials within a rule block) and quickly destabilized after changing to the other rule
358 (**Figure 3A**). We adopted a newly developed dimensionality-reduction method CEBRA
359 (Schneider et al., 2023), utilizing contrastive learning to visualize the difference of high-

360 dimensional neural data across rules. For a common trajectory across the two rules (*Left-to-*
361 *Center*), PFC 3D embeddings using CEBRA qualitatively showed consistent separation across
362 rules for all animals during stable performance (visualized in **Figure 3B (ii)**, top row). These
363 embeddings used training and test datasets within animals. We also used multi-session training
364 that sampled training data from all animals followed by testing within animals. The embeddings
365 from this method revealed a similar structure across animals, implying animal-invariant features
366 in the PFC ensemble data for rule representations (**Figure 3B (ii)**, bottom row). CA1 single-
367 session embeddings showed similar separations between rules compared to PFC. However,
368 much weaker separations were observed in multi-animal embeddings, suggesting a more
369 unique latent space of CA1 rule-specific activity for individual animals (**Figure 3B (i)**). As
370 animals switched from stable performance of one rule to another, we also observed a
371 systematic transition in the manifold space (example PFC manifold transitions over trials in
372 **Figure 3C**).
373 In order to quantify these changes, a KNN decoder was trained to decode the underlying rule
374 using single-animal embeddings for each brain region (see **Materials and Methods**). Rule
375 decoding probabilities using CA1 and PFC data correlated highly with animals' behavior strategy
376 (**Figure 3D, E**). Upon further inspection, behavior strategy showed stronger correlation with
377 PFC rule decoding than with CA1 decoding (**Figure 3E**). The decoding probability of the current
378 rule increased with behavioral performance for both PFC and CA1 (**Figure 3F**, mean decoding
379 accuracy for low performance: CA1 0.38, PFC 0.41; mid performance: CA1 0.66, PFC 0.71;
380 high performance: CA1 0.97, PFC 0.96; performance thresholds are reported in **Materials and**
381 **Methods**). However, when training the decoder using multi-animal embeddings, CA1
382 ensembles performed much worse than PFC, again implying more consistent rule coding across
383 animals in PFC and its stronger relevance to behavior than CA1 (**Figure 3F**).
384 We further examined the timing between neural representation change and behavior strategy
385 shift upon rule switch. The behavior and neural changes align with each other, with neural

386 representations in both CA1 and PFC transitioned more often before behavior strategy than
387 after (**Figure 3H, I**), with no timing difference seen between CA1 and PFC ensembles. On
388 average, it took more trials to switch from rule 1 to rule 2, both in the neural representation and
389 behaviorally (**Figure 3G**), potentially due to asymmetric working memory components in rule 2.
390

391 **VTA DA firing activity reflects and predicts reward outcomes**

392 As midbrain DA plays a crucial role in reward signaling, we aimed to understand VTA DA
393 spiking activity features during rapid rule switches guided by unexpected reward outcomes. We
394 used an opto-tagging strategy in TH-Cre rats, which has been utilized in previous studies
395 (Witten et al., 2011). Opto-tagging was performed during the first or last sleep session for each
396 day of recording to not interfere with activity during task running. We recorded a total of 53 VTA
397 neurons, out of which 20 photo-tagged cells were identified as putative DA neurons (with firing
398 rates, mean ± std, 7.7 ± 3.0 Hz). Consistent with a vast body of literature, putative DA neurons
399 showed increased firing rates when rewards became available, temporally aligned to first poke
400 at reward well, and decreased firing rates during reward omission (**Figure 4A,** median z-scored
401 firing rate for rewarded trials: 0.49, unrewarded trials: -0.76, $p = 5.6\times10^{-5}$ Wilcoxon signed rank
402 test). Non-tagged neurons exhibited a diverse range of activity, including 45.5% (15/33) of
403 neurons responding to reward outcomes (**Figure 4B**). Further, we also observed that DA
404 neurons had higher firing rates during running for trials that lead to rewards in comparison to
405 unrewarded trials (**Figure 4C**, median z-scored firing rate for rewarded trials: 0.11, unrewarded
406 trials: -0.060, $p = 1.8\times10^{-4}$). This difference became apparent and significant halfway through
407 running on the trajectory, just after the choice point where the decision was made, similar to
408 previous findings of DA release in striatum, and is likely related to reward expectancy/
409 uncertainty (Howe et al., 2013). The running speed profile on the track was similar between
410 rewarded and unrewarded trials, suggesting the DA firing rate difference is not caused by a
411 change in motivation or vigor (**Figure 4D**).

412 Based on the proposed link between DA spiking and reward prediction error, it is predicted
413 that for rewarded trials, as behavioral performance improves, DA firing rates at the reward will
414 decrease and DA firing rates during run will increase; and such trends would be the opposite for
415 unrewarded trials (Watabe-Uchida et al., 2017). However, we observed a strong positive
416 correlation between run and reward firing rates ($r = 0.60$, $p = 6.8\times10^{-148}$), and no obvious
417 relationship between firing rates of either state to performance (**Figure 4E**). We further tested
418 this by separating the performance by trials into low and high performance halves, and found no
419 difference in the firing rates across performance stages for either rewarded or unrewarded trials
420 (n=20 cells, median z-scored firing rate for rewarded trials: run: low performance 0.065, high
421 performance 0.13, p=0.23; outcome: low performance 0.54, high performance 0.44, p=1.00;
422 unrewarded trials: run: low performance -0.072, high performance -0.049, p=0.23; outcome: low
423 performance -0.81, high performance -0.71, p=0.65, Wilcoxon paired rank test, **Figure 4F**).
424 In addition, we wanted to investigate if the DA reward prediction signal is present for working
425 memory error as compared to rule/perseverative error that occurs after a rule switch. At each
426 time of rule switching, two trajectories became unrewarding under all conditions and two new
427 ones became potentially rewarding when the sequence of arm visits was correct. For example,
428 when rule 1 changes to rule 2, trajectories between the center and the right arms are no longer
429 rewarding. Instead, left-to-right and right-to-left ones yield rewards. We classified the trials that
430 animals ran on the newly unrewarding trajectories as perseverative errors, whereas the trials
431 that animals made a wrong outbound choice for the current rule as working memory errors. If
432 the DA firing activity only reflects a model-free system tracking overall reward probability, we
433 would expect a difference only between perseverative errors and correct trials, but not for
434 individual decisions dependent on working memory. We found that the prediction for reward
435 outcome was present in DA firing regardless of the error type, even when comparing error trials
436 to nearest correct trials of the same outbound/inbound trajectory type (**Figure 4G**, median z-

437 scored firing rate difference between rewarded and unrewarded trials: outbound 0.12, p =
438 1.0×10^{-13}, n = 217 trials; inbound 0.085, p = 1.8×10^{-6}, n = 178 trials).
439 To summarize the influence of reward conditions and histories on DA firing rates, we fitted
440 multi-regression models for each cell's spiking rates during running and outcome periods,
441 separately. The most significant factor was found to be the current trial's reward outcome
442 (running: mean±sem coefficients: 0.14±0.02, significant for 65% of DA neurons; outcome:
443 0.95±0.13, 95%), in comparison to a weaker impact of reward history (running: 0.11±0.10, 45%;
444 outcome: -0.13±0.16, 30%) or same-trajectory reward history (running: 0.074±0.058, 30%;
445 outcome: -0.39±0.07, 65%), for both running and reward states (**Figure 4H**). Note that current
446 trial reward outcome is a significant contributor to the approach run firing rate, and not just for
447 reward well firing rate that is expected.
448
449 **DA reward predicting feature develops after rule switching and coordinates with PFC rule**
450 **representation transition before behavior strategy adaptation**
451 Our findings in PFC/CA1 rule coding and DA reward signals led us to the question -- if the
452 firing rates of DA neurons predictive of reward outcomes develop as animals gather evidence of
453 a rule change. Firing rates upon reward delivery were consistently higher than at reward
454 omission (**Figure 5A (iv)**); however, the difference in DA neuron firing between rewarded and
455 unrewarded trials during running only developed a few trials after the rule switch was
456 implemented (**Figure 5A (v)**), and a few trials prior to behavioral strategy switch (**Figure 5A (i)**).
457 We further investigated whether this DA firing activity is coordinated with rule representation
458 changes in CA1 and PFC. When aligned to the trial where PFC started to decode the current
459 rule, DA firing rate difference during run between rewarded and unrewarded trials ramped up
460 robustly toward this change point (**Figure 5B**, bottom). The ramp up in DA firing rate difference
461 was qualitatively more robust and consistent for PFC representation switch rather than when
462 aligned to CA1 representation switch (**Figure 5C**, bottom). Animals' behavior strategies adapted

accordingly shortly after (on average 4 trials) the observed PFC rule representation switch and DA prediction emergence (**Figure 5B,** top). In addition, the DA firing activity difference between rewarded and unrewarded trials during maze running did not stay high as animals reached good, stable performance for the new rule. We observed a positive correlation between the DA firing rate difference and the rate of PFC decoding probability change, which may suggest a gating mechanism of value/belief update (**Figure 5D**). In summary, the reward predictive/expectancy property of DA firing during running is acquired post rule switch and is coordinated with the changes of PFC rule representation and behavior strategy.

Discussion

In the current study, we examined rule-related firing properties in the hippocampus and PFC, VTA DA spiking activity during rule switching, and the temporal relationships between cognitive rule representation, reward prediction signal and behavior adaptation. The mechanisms of rule representation and reward prediction have been generally examined separately, but it is vital to gain an integrated understanding of dynamics and temporal coordination between these mechanisms for supporting cognitive flexibility and behavioral adaptation. During rule switching, the presence or absence of rewards after specific actions can serve as feedback for organisms to reevaluate their behavior policy. A conflict between belief and outcome leads to a switch in internal rule representations, which can guide correct behavioral actions for the changed context. We therefore reasoned that there must exist some sort of temporal coordination between reward prediction and rule representation dynamics over the course of a few trials after rule switching, which will determine the time course of behavioral adjustments, thus allowing animals to overcome perseveration and adapt to the new context with appropriate actions. We found that PFC and hippocampal CA1 population activity represented rule context. VTA DA firing activity responded to and predicted reward outcomes. The timings of the switches in PFC-CA1 rule representation and the emergence of correct reward prediction from VTA were coordinated. Further, these changes in PFC, CA1 and VTA DA firing activity led the behavioral strategy transition, suggesting coordinated network activity switches to support behavioral adaptation.

We implemented a spatial rule switching task in a W/M maze, probing behavioral flexibility and working memory at the same time in the exact same environment. Rule 1 comprises a traditional W-maze alternation rule with the center arm as home arm as in previous studies (Frank et al., 2000; Jadhav et al., 2012, 2016; Tang et al., 2017; Maharjan et al., 2018; Shin et al., 2019), and the home arm switched to the left arm for Rule 2, requiring the animals to change their strategy for optimal trajectory sequences across the rules. Notably, both rules incorporate a

498 spatial working memory component (outbound component), requiring the animals to choose the
499 opposite arm from previous choice when embarking from the home arm. The return-to-home-
500 arm trajectory is the inbound component with a spatial reference memory demand (Kim and
501 Frank, 2009). The nature of the task assigned different memory demands of overlapping
502 trajectories in the two rules, which allowed us to compare animal behavior, CA1/PFC
503 representations and DA signaling for reward prediction during rule switch.

504 We first examined the differences of rule representation between the hippocampal CA1 and
505 PFC. Spiking activity changes associated with rule/context were observed in both brain regions
506 (Guise and Shapiro, 2017; Hasz and Redish, 2020), with single neurons exhibiting remapping
507 on the same trajectories across the two rule contexts. Examining ensemble coding using
508 manifold analysis and decoding to current rule context revealed more robust and consistent
509 coding of rule contexts across animals in PFC, suggesting that similar neural representations
510 may develop in PFC to support two rule contexts in the same physical trajectory space on
511 mazes. Rule representations in PFC appeared to shift over the course of a few to tens of trials
512 after rule switching, prior to observation of a behavioral strategy switch.

513 We observed more consistency across animals in PFC ensemble decoding for rules, whereas
514 CA1 ensemble representations were more animal-specific (**Fig. 3B**). In terms of timing, we did
515 not see a significant difference between PFC and CA1 in terms of neural transition times as
516 compared with behavioral transition times, in terms of number of trials, although there was some
517 variability across regions (**Fig. 3H, I**). However, the DA prediction differences that emerged after
518 rule changes were more robustly aligned to PFC transition times than to CA1 (**Fig. 5B-C**), and
519 PFC transition times were more closely aligned to behavioral strategy switch (**Fig. 3E**).
520 Therefore, although there were no significant timing differences between PFC and CA1, this
521 suggests more consistency in PFC neural transitions and behavioral transitions.

522 We observed that VTA DA neurons participated in reward prediction and this rule-specific
523 feature developed quickly after rule switching. Previous literature has often focused on model-

free RL reward prediction error; here, we instead tried to understand how midbrain DA neuronal firing activity changes during a rule switching task that requires working memory. DA neuronal firing rates were highly correlated between running and reward outcome in a trial, which somewhat resembles previous findings in (Coddington and Dudman, 2018). In addition, we did not find a correlation between DA spiking activity and performance at the population level. These results contrast with the prediction based on classical conditioning that firing activity increases toward cue/beginning of a trial and slowly diminishes upon reward delivery (Schultz et al., 1997; Fiorillo et al., 2003; Amo et al., 2022). Rather, our findings suggest that DA signaling may incorporate rule-based and working-memory dependent prediction information, potentially from cortical input.

We found a delay in animals' behavioral strategy adjustment in comparison to rule representation and reward prediction. Animals continued to sample from wrong trajectories, although at a lower frequency, after manifolds shifted to the new rule and DA signal could predict the reward outcome. This can be explained by simply reserving a small chance for random exploration, or perhaps by the theory of active inference (Friston et al., 2012, 2014). In this theory, the dopamine signal minimizes surprise instead of cost. Therefore, sampling from extra trials could help confirm animals' beliefs if correct and eventually stabilize behavioral sequences.

How is information processed in these regions? Does VTA receive reward, expectation or reward prediction error (RPE) information from other regions? Lisman and Grace (2005) suggested that novelty information is conveyed to VTA from the hippocampal formation through an indirect route, possibly with inhibitory afferents from accumbens and ventral pallidum. In return, DA fibers innervate dorsal hippocampus and thus enhance LTP (Huang and Kandel, 1995; Otmakhova and Lisman, 1996; Li et al., 2003; Rosen et al., 2015; Sayegh et al., 2024). In terms of DA-cortical interactions, VTA receives abundant prefrontal glutamatergic projections (Geisler et al., 2007), and their impact on reward signaling is multifaceted. Input from frontal

550 cortices is critical for conveying predictive and incentive features of a cue (Pan et al., 2021).
551 PFC conveys belief state information to the dopaminergic system and affects RPE computation
552 when hidden states are involved (Babayan et al., 2018; Starkweather et al., 2018). Additionally,
553 Amo et al. (2024) showed glutamatergic input to VTA already carried RPE signal, challenging
554 the classic view of local computation of RPE in VTA by combining different aspects of reward
555 and expectation from glutamatergic and GABAergic inputs (Kawato and Samejima, 2007; Keiflin
556 and Janak, 2015). An intriguing future direction of research could focus on dissecting
557 computational features or components of RPE in these brain regions involved in the reward
558 circuit, particularly when multiple cognitive demands are present.
559 It is important to differentiate between DA firing activity and DA release in downstream area.
560 We did not observe an obvious increase in DA spiking activity during goal approach. However,
561 downstream release in striatum has been reported to ramp up towards goal (Howe et al., 2013;
562 Hamid et al., 2015), suggesting partially dissociated activity potentially caused by local
563 modulation (Mohebi et al., 2019). It would be interesting to examine if the working-memory
564 dependent reward prediction signal is present in the DA release profile as in VTA DA spiking
565 activity, and if so, how that influences its downstream striatal and cortical areas.
566 The exact mechanism of information transfer and cooperation requires further investigation.
567 For example, Fujisawa and Buzsáki (2011) proposed a 4 Hz rhythm orchestrating neuronal
568 activity in the hippocampus, PFC and VTA during a similar working memory task. DA
569 administration in PFC increased HPC-PFC theta coherence and PFC phase locking to CA1
570 theta (Benchenane et al., 2010). PFC theta sequences selectively coordinate with CA1 theta
571 sequences depicting future trajectory choices (Tang et al., 2021). Therefore, altered DA neuron
572 spiking activity might be impacted by the online processes of action evaluation and selection
573 during running. Another possible mechanism is through coordinated reactivation/replay. It has
574 been shown that hippocampal reactivation is associated with increased firing activity of VTA
575 cells as a potential mechanism for memory consolidation (Gomperts et al., 2015). CA1-PFC

coordinated replay is biased toward behavioral choice and therefore can potentially participate in working memory and decision making (Shin et al., 2019). This hippocampo-cortical/subcortical temporal coordination during offline states may serve as substrates for value updates, memory consolidation, action evaluation and planning. Our study focused on the behavioral time scale, but investigating simultaneous activity on a shorter time scale (50-200 ms) can potentially uncover detailed mechanisms of inter-regional communication.

Conclusions

To understand the temporal coordination between cognitive systems and reward systems, we recorded from the rat hippocampal CA1, PFC and VTA during a rapid rule switching task. CA1 and PFC exhibited rule representation in their population activity. DA neuron firing activity in VTA gradually became predictive of reward outcomes after rule switching, and this predictive feature developed together with the PFC representation transition to reflect the new rule. These neural representations changed in advance of behavioral adaptation by a few trials. Together, our study revealed a synchronized update of information across PFC, HPC and VTA that potentially supports behavioral flexibility.

References

Amo R, Matias S, Yamanaka A, Tanaka KF, Uchida N, Watabe-Uchida M (2022) A gradual temporal shift of dopamine responses mirrors the progression of temporal difference error in machine learning. Nature Neuroscience 2022:1–11.

Amo R, Uchida N, Watabe-Uchida M (2024) Glutamate inputs send prediction error of reward, but not negative value of aversive stimuli, to dopamine neurons. Neuron 112:1001-1019.e6.

Babayan BM, Uchida N, Gershman SJ (2018) Belief state representation in the dopamine system. Nature Communications 2018 9:1 9:1–10.

Barthó P, Hirase H, Monconduit L, Zugaro M, Harris KD, Buzsáki G (2004) Characterization of neocortical principal cells and interneurons by network interactions and extracellular features. J Neurophysiol 92:600–608.

Beier KT, Steinberg EE, Deloach KE, Xie S, Miyamichi K, Schwarz L, Gao XJ, Kremer EJ, Malenka RC, Luo L (2015) Circuit Architecture of VTA Dopamine Neurons Revealed by Systematic Input-Output Mapping. Cell 162:622–634.

Benchenane K, Peyrache A, Khamassi M, Tierney PL, Gioanni Y, Battaglia FP, Wiener SI (2010) Coherent Theta Oscillations and Reorganization of Spike Timing in the Hippocampal-Prefrontal Network upon Learning. Neuron 66:921–936.

Carr DB, Sesack SR (2000) Projections from the Rat Prefrontal Cortex to the Ventral Tegmental Area: Target Specificity in the Synaptic Associations with Mesoaccumbens and Mesocortical Neurons. Journal of Neuroscience 20:3864–3873.

Chung JE, Magland JF, Barnett AH, Tolosa VM, Tooker AC, Lee KY, Shah KG, Felix SH, Frank LM, Greengard LF (2017) A Fully Automated Approach to Spike Sorting. Neuron 95:1381-1394.e6.

Coddington LT, Dudman JT (2018) The timing of action determines reward prediction signals in identified midbrain dopamine neurons. Nature Neuroscience 2018 21:11 21:1563–1573.

Cohen JY, Haesler S, Vong L, Lowell BB, Uchida N (2012) Neuron-type-specific signals for reward and punishment in the ventral tegmental area. Nature 2012 482:7383 482:85–88.

Dabney W, Kurth-Nelson Z, Uchida N, Starkweather CK, Hassabis D, Munos R, Botvinick M (2020) A distributional code for value in dopamine-based reinforcement learning. Nature 2020 577:7792 577:671–675.

Durstewitz D, Vittoz NM, Floresco SB, Seamans JK (2010) Abrupt Transitions between Prefrontal Neural Ensemble States Accompany Behavioral Transitions during Rule Learning. Neuron 66:438–448.

Engelhard B, Finkelstein J, Cox J, Fleming W, Jang HJ, Ornelas S, Koay SA, Thiberge SY, Daw ND, Tank DW, Witten IB (2019) Specialized coding of sensory, motor and cognitive variables in VTA dopamine neurons. Nature 2019 570:7762 570:509–513.

Eschenko O, Mizumori SJY (2007) Memory influences on hippocampal and striatal neural codes: Effects of a shift between task rules. Neurobiol Learn Mem 87:495–509.

Ferbinteanu J, Shirvalkar P, Shapiro ML (2011) Memory Modulates Journey-Dependent Coding in the Rat Hippocampus. Journal of Neuroscience 31:9135–9146.

Fiorillo CD, Tobler PN, Schultz W (2003) Discrete coding of reward probability and uncertainty by dopamine neurons. Science (1979) 299:1898–1902.

Frank LM, Brown EN, Wilson M (2000) Trajectory encoding in the hippocampus and entorhinal cortex. Neuron 27:169–178.

Friston K, Schwartenbeck P, FitzGerald T, Moutoussis M, Behrens T, Dolan RJ (2014) The anatomy of choice: dopamine and decision-making. Philosophical Transactions of the Royal Society B: Biological Sciences 369.

Friston KJ, Shiner T, FitzGerald T, Galea JM, Adams R, Brown H, Dolan RJ, Moran R, Stephan KE, Bestmann S (2012) Dopamine, Affordance and Active Inference. PLoS Comput Biol 8:e1002327.

Fujisawa S, Buzsáki G (2011) A 4 Hz Oscillation Adaptively Synchronizes Prefrontal, VTA, and Hippocampal Activities. Neuron 72:153–165.

Gasbarri A, Packard MG, Campana E, Pacitti C (1994) Anterograde and retrograde tracing of projections from the ventral tegmental area to the hippocampal formation in the rat. Brain Res Bull 33:445–452.

Gauthier JL, Tank DW (2018) A Dedicated Population for Reward Coding in the Hippocampus. Neuron 99:179-193.e7.

Geisler S, Derst C, Veh RW, Zahm DS (2007) Glutamatergic Afferents of the Ventral Tegmental Area in the Rat. Journal of Neuroscience 27:5730–5743.

Gomperts SN, Kloosterman F, Wilson MA (2015) VTA neurons coordinate with the hippocampal reactivation of spatial experience. Elife 4.

Griffin AL, Eichenbaum H, Hasselmo ME (2007) Spatial Representations of Hippocampal CA1 Neurons Are Modulated by Behavioral Context in a Hippocampus-Dependent Memory Task. Journal of Neuroscience 27:2416–2423.

Guise KG, Shapiro ML (2017) Medial Prefrontal Cortex Reduces Memory Interference by Modifying Hippocampal Encoding. Neuron 94:183-192.e8.

Hamid AA, Pettibone JR, Mabrouk OS, Hetrick VL, Schmidt R, Vander Weele CM, Kennedy RT, Aragona BJ, Berke JD (2015) Mesolimbic dopamine signals the value of work. Nature Neuroscience 2016 19:1 19:117–126.

Hasz BM, Redish AD (2020) Dorsomedial prefrontal cortex and hippocampus represent strategic context even while simultaneously changing representation throughout a task session. Neurobiol Learn Mem 171:107215.

Horst NK, Laubach M (2009) The role of rat dorsomedial prefrontal cortex in spatial working memory. Neuroscience 164:444–456.

Howe MW, Tierney PL, Sandberg SG, Phillips PEM, Graybiel AM (2013) Prolonged dopamine signalling in striatum signals proximity and value of distant rewards. Nature 2013 500:7464 500:575–579.

Huang YY, Kandel ER (1995) D1/D5 receptor agonists induce a protein synthesis-dependent late potentiation in the CA1 region of the hippocampus. Proceedings of the National Academy of Sciences 92:2446–2450.

Hyman JM, Ma L, Balaguer-Ballester E, Durstewitz D, Seamans JK (2012) Contextual encoding by ensembles of medial prefrontal cortex neurons. Proc Natl Acad Sci U S A 109:5086–5091.

Hyman JM, Zilli EA, Paley AM, Hasselmo ME (2010) Working memory performance correlates with prefrontal-hippocampal theta interactions but not with prefrontal neuron firing rates. Front Integr Neurosci 4:1162.

Jadhav SP, Kemere C, German PW, Frank LM (2012) Awake hippocampal sharp-wave ripples support spatial memory. Science (1979) 336:1454–1458.

Jadhav SP, Rothschild G, Roumis DK, Frank LM (2016) Coordinated Excitation and Inhibition of Prefrontal Ensembles during Awake Hippocampal Sharp-Wave Ripple Events. Neuron 90:113–127.

Kabanova A, Pabst M, Lorkowski M, Braganza O, Boehlen A, Nikbakht N, Pothmann L, Vaswani AR, Musgrove R, Di Monte DA, Sauvage M, Beck H, Blaess S (2015) Function and developmental origin of a mesocortical inhibitory circuit. Nature Neuroscience 2015 18:6 18:872–882.

Karlsson MP, Tervo DGR, Karpova AY (2012) Network resets in medial prefrontal cortex mark the onset of behavioral uncertainty. Science (1979) 338:135–139.

Kawato M, Samejima K (2007) Efficient reinforcement learning: computational theories, neuroscience and robotics. Curr Opin Neurobiol 17:205–212.

692 Keiflin R, Janak PH (2015) Dopamine Prediction Errors in Reward Learning and Addiction: From
693 Theory to Neural Circuitry. Neuron 88:247–263.
694 Kim HGR, Malik AN, Mikhael JG, Bech P, Tsutsui-Kimura I, Sun F, Zhang Y, Li Y, Watabe-Uchida
695 M, Gershman SJ, Uchida N (2020) A Unified Framework for Dopamine Signals across
696 Timescales. Cell 183:1600-1616.e25.
697 Kim SM, Frank LM (2009) Hippocampal Lesions Impair Rapid Learning of a Continuous Spatial
698 Alternation Task Tanimoto H, ed. PLoS One 4:e5494.
699 Krausz TA, Comrie AE, Kahn AE, Frank LM, Daw ND, Correspondence JDB, Berke JD (2023)
700 Dual credit assignment processes underlie dopamine signals in a complex spatial
701 environment. Neuron 111:3465–3478.
702 Krishnan S, Heer C, Cherian C, Sheffield MEJ (2022) Reward expectation extinction
703 restructures and degrades CA1 spatial maps through loss of a dopaminergic reward
704 proximity signal. Nature Communications 2022 13:1 13:1–19.
705 Kvitsiani D, Ranade S, Hangya B, Taniguchi H, Huang JZ, Kepecs A (2013) Distinct behavioural
706 and network correlates of two interneuron types in prefrontal cortex. Nature 498:363–366.
707 Lak A, Okun M, Moss MM, Gurnani H, Farrell K, Wells MJ, Reddy CB, Kepecs A, Harris KD,
708 Carandini M (2020) Dopaminergic and Prefrontal Basis of Learning from Sensory
709 Confidence and Reward Value. Neuron 105:700-711.e6.
710 Lee H, Ghim JW, Kim H, Lee D, Jung MW (2012) Hippocampal Neural Correlates for Values of
711 Experienced Events. Journal of Neuroscience 32:15053–15065.
712 Li S, Cullen WK, Anwyl R, Rowan MJ (2003) Dopamine-dependent facilitation of LTP induction
713 in hippocampal CA1 by exposure to spatial novelty. Nature Neuroscience 2003 6:5 6:526–
714 531.
715 Lisman JE, Grace AA (2005) The Hippocampal-VTA Loop: Controlling the Entry of Information
716 into Long-Term Memory. Neuron 46:703–713.

717 Ma L, Hyman JM, Durstewitz D, Phillips AG, Seamans JK (2016) A Quantitative Analysis of
718 Context-Dependent Remapping of Medial Frontal Cortex Neurons and Ensembles. Journal
719 of Neuroscience 36:8258–8272.
720 Maharjan DM, Dai YY, Glantz EH, Jadhav SP (2018) Disruption of dorsal hippocampal –
721 prefrontal interactions using chemogenetic inactivation impairs spatial learning. Neurobiol
722 Learn Mem 155:351–360.
723 Martig AK, Mizumori SJY (2011) Ventral tegmental area disruption selectively affects CA1/CA2
724 but not CA3 place fields during a differential reward working memory task. Hippocampus
725 21:172–184.
726 McNamara CG, Tejero-Cantero Á, Trouche S, Campo-Urriza N, Dupret D (2014) Dopaminergic
727 neurons promote hippocampal reactivation and spatial memory persistence. Nat Neurosci
728 17:1658–1660.
729 Mohebi A, Pettibone JR, Hamid AA, Wong J-MT, Vinson LT, Patriarchi T, Tian L, Kennedy RT,
730 Berke JD (2019) Dissociable dopamine dynamics for learning and motivation. Nature 2019
731 570:7759 570:65–70.
732 Morales M, Margolis EB (2017) Ventral tegmental area: Cellular heterogeneity, connectivity and
733 behaviour. Nat Rev Neurosci 18:73–85.
734 O'Keefe J (1978) The hippocampus as a cognitive map. Oxford University Press.
735 O'Keefe J, Dostrovsky J (1971) The hippocampus as a spatial map. Preliminary evidence from
736 unit activity in the freely-moving rat. Brain Res 34:171–175.
737 Otmakhova NA, Lisman JE (1996) D1/D5 Dopamine Receptor Activation Increases the
738 Magnitude of Early Long-Term Potentiation at CA1 Hippocampal Synapses. Journal of
739 Neuroscience 16:7478–7486.
740 Pan WX, Coddington LT, Dudman JT (2021) Dissociable contributions of phasic dopamine
741 activity to reward and prediction. Cell Rep 36:109684.

Powell NJ, Redish AD (2016) Representational changes of latent strategies in rat medial prefrontal cortex precede changes in behaviour. Nature Communications 2016 7:1 7:1–11.

Ragozzino ME, Kesner RP (1998) The Effects of Muscarinic Cholinergic Receptor Blockade in the Rat Anterior Cingulate and Prelimbic/Infralimbic Cortices on Spatial Working Memory. Neurobiol Learn Mem 69:241–257.

Rich EL, Shapiro M (2009) Rat Prefrontal Cortical Neurons Selectively Code Strategy Switches. Journal of Neuroscience 29:7208–7219.

Roesch MR, Calu DJ, Schoenbaum G (2007) Dopamine neurons encode the better option in rats deciding between differently delayed or sized rewards. Nature Neuroscience 2007 10:12 10:1615–1624.

Rosen ZB, Cheung S, Siegelbaum SA (2015) Midbrain dopamine neurons bidirectionally regulate CA3-CA1 synaptic drive. Nature Neuroscience 2015 18:12 18:1763–1771.

Sayegh FJP, Mouledous L, Macri C, Pi Macedo J, Lejards C, Rampon C, Verret L, Dahan L (2024) Ventral tegmental area dopamine projections to the hippocampus trigger long-term potentiation and contextual learning. Nature Communications 2024 15:1 15:1–12.

Schneider S, Lee JH, Mathis MW (2023) Learnable latent embeddings for joint behavioural and neural analysis. Nature 2023 617:7960 617:360–368.

Schultz W, Apicella P, Ljungberg T (1993) Responses of monkey dopamine neurons to reward and conditioned stimuli during successive steps of learning a delayed response task. Journal of Neuroscience 13:900–913.

Schultz W, Dayan P, Montague PR (1997) A neural substrate of prediction and reward. Science (1979) 275:1593–1599.

Shin JD, Jadhav SP (2024) Prefrontal cortical ripples mediate top-down suppression of hippocampal reactivation during sleep memory consolidation. Current Biology 34:2801-2811.e9.

Shin JD, Tang W, Jadhav SP (2019) Dynamics of Awake Hippocampal-Prefrontal Replay for Spatial Learning and Memory-Guided Decision Making. Neuron.

Sirota A, Montgomery S, Fujisawa S, Isomura Y, Zugaro M, Buzsáki G (2008) Entrainment of Neocortical Neurons and Gamma Oscillations by the Hippocampal Theta Rhythm. Neuron 60:683–697.

Skaggs WE, Mcnaughton BL, Gothard KM (1992) An Information-Theoretic Approach to Deciphering the Hippocampal Code. Adv Neural Inf Process Syst 5.

Smith AC, Frank LM, Wirth S, Yanike M, Hu D, Kubota Y, Graybiel AM, Suzuki WA, Brown EN (2004) Dynamic analysis of learning in behavioral experiments. J Neurosci 24:447–461.

Starkweather CK, Gershman SJ, Uchida N (2018) The Medial Prefrontal Cortex Shapes Dopamine Reward Prediction Errors under State Uncertainty. Neuron 98:616-629.e6.

Steinberg EE, Keiflin R, Boivin JR, Witten IB, Deisseroth K, Janak PH (2013) A causal link between prediction errors, dopamine neurons and learning. Nat Neurosci 16:966–973.

Tang W, Shin JD, Frank LM, Jadhav SP (2017) Hippocampal-Prefrontal Reactivation during Learning Is Stronger in Awake Compared with Sleep States. J Neurosci 37:11789–11805.

Tang W, Shin JD, Jadhav SP (2021) Multiple time-scales of decision-making in the hippocampus and prefrontal cortex. Elife 10.

Urban KR, Layfield DM, Griffin AL (2014) Transient inactivation of the medial prefrontal cortex impairs performance on a working memory-dependent conditional discrimination task. Behavioral Neuroscience 128:639–643.

Watabe-Uchida M, Eshel N, Uchida N (2017) Neural Circuitry of Reward Prediction Error. Annu Rev Neurosci 40:373–394.

Witten IB, Steinberg EE, Lee SY, Davidson TJ, Zalocusky KA, Brodsky M, Yizhar O, Cho SL, Gong S, Ramakrishnan C, Stuber GD, Tye KM, Janak PH, Deisseroth K (2011) Recombinase-driver rat lines: Tools, techniques, and optogenetic application to dopamine-mediated reinforcement. Neuron 72:721–733.

Wood ER, Dudchenko PA, Robitsek RJ, Eichenbaum H (2000) Hippocampal neurons encode information about different types of memory episodes occurring in the same location. Neuron 27:623–633.

Yoon T, Okada J, Jung MW, Kim JJ (2008) Prefrontal cortex and hippocampus subserve different components of working memory in rats. Learning & Memory 15:97–105.

Zielinski MC, Shin JD, Jadhav SP (2019) Coherent Coding of Spatial Position Mediated by Theta Oscillations in the Hippocampus and Prefrontal Cortex. Journal of Neuroscience 39:4550–4565.

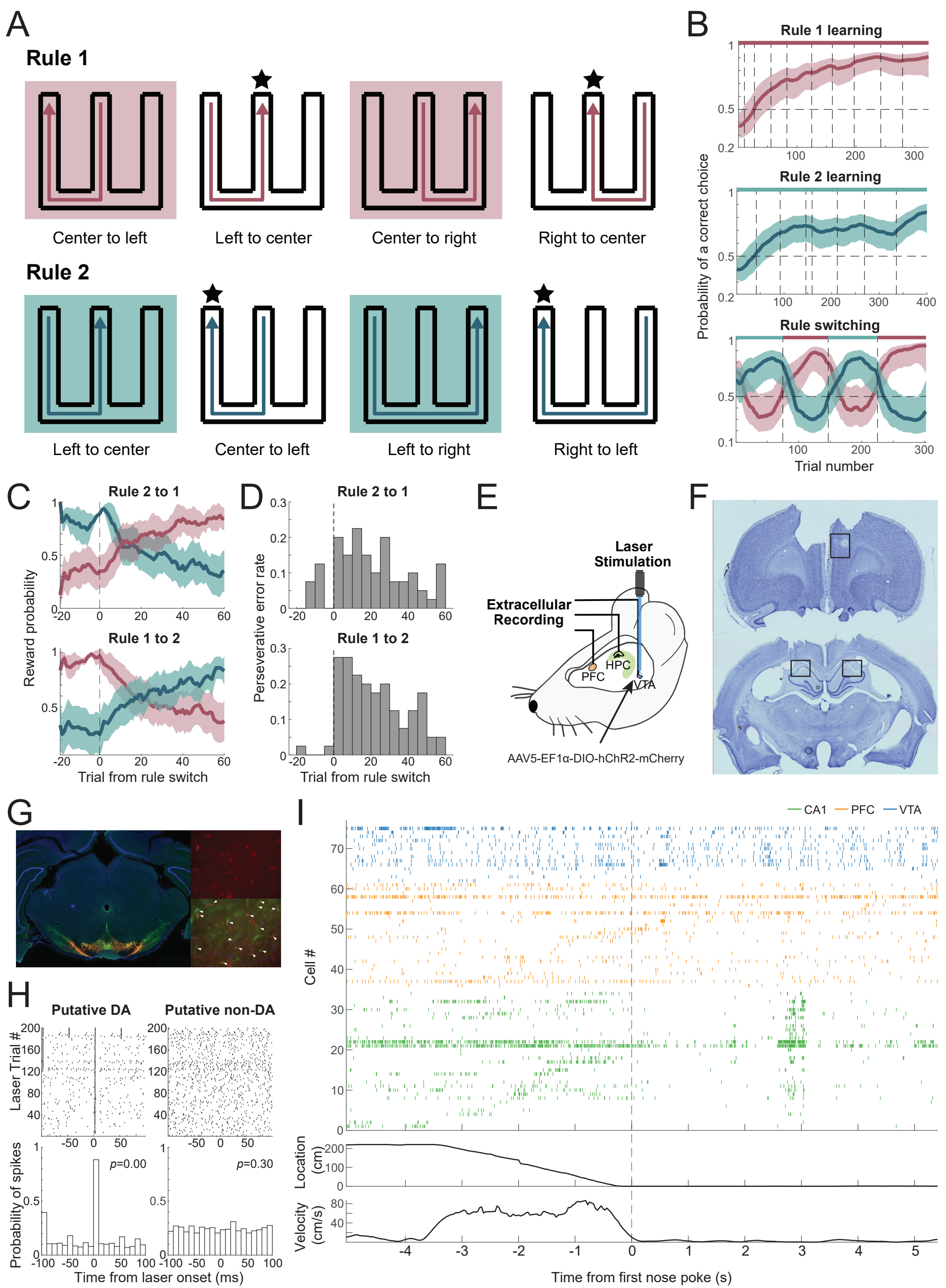
A
Rule 1
Center to left
Left to center
Center to right
Right to center
Rule 2
Left to center
Center to left
Left to right
Right to left
B
Rule 1 learning
Rule 2 learning
Rule switching
Probability of a correct choice
Trial number
C
Rule 2 to 1
Rule 1 to 2
Reward probability
Trial from rule switch
D
Rule 2 to 1
Rule 1 to 2
Perseverative error rate
Trial from rule switch
E
Laser Stimulation
Extracellular Recording
HPC
PFC
VTA
AAV5-EF1α-DIO-hChR2-mCherry
F
G
H
Putative DA
Putative non-DA
Laser Trial #
Probability of spikes
p=0.00
p=0.30
Time from laser onset (ms)
I
CA1
PFC
VTA
Cell #
Location (cm)
Velocity (cm/s)
Time from first nose poke (s)

Fig 1: Behavior and Recording Paradigm.

A. W-track rule-switching behavior. Top: sequence of rule 1, left-center-right-center; bottom: sequence of rule 2, center-left-right-left. Stars denote the home arm in the given rule sequence. Trajectories in shaded boxes are outbound and require working memory. The common trajectories across the two rules are Left-to-Center and Center-to-Left, with different memory demands for the rules.

B. Example performance curve of one animal (estimated mean ± 95% CI). *Left*: Rule 1 learning across behavior epochs/ sessions; *Middle*: Rule 2 learning; *Right*: rapid switching between the two rules within a single day. Note that the rule switch is not indicated by any external cue. The bar on top indicates the current rule (dark red for rule 1, teal for rule 2). Dashed lines in all three panels indicate epoch changes.

C. Average reward rate of behavioral choices based on each rule's reward contingency, for Rule 2 to 1 and Rule 1 to 2 switches separately (n=8 each), aligned to rule switch trials.

D. Probability of perseverative error aligned to rule switch trials, for Rule 2 to 1 and Rule 1 to 2 respectively.

E. Recording setup. Simultaneous recording in dCA1, mPFC and VTA regions during rule switching behavior, with photo-tagging of TH+ neurons in the VTA in TH-Cre animals.

F. Example of Nissl-stained PFC and CA1 slices. Rectangles indicate regions of lesion marks.

G. Histology in VTA. Red: virus expression of AAV5-EF1a-DIO-hChR2(E123T/T159C)-mCherry; green: antibody staining of TH+ cells; blue: DAPI. White triangles show overlap between virus expression and antibody staining.

H. VTA spiking responses to laser stimulation at 0 ms. Top: raster plot showing individual spikes aligned to each stimulation onset. Bottom: probability of spiking. Left: example of an opto-tagged neuron (p=0); right: example non-tagged VTA neuron (p=0.30, Stimulus-Associated spike Latency Test, SALT).

I. Top: spike raster during an example trial starting with the animal leaving the last reward location, running a trajectory to the next reward, followed by immobility and consumption at new reward location. Green: CA1 cells; orange: PFC; blue: VTA. Middle: linear distance to reference reward location. Bottom: movement speed. Dashed line: time of first nose poke at the destination reward location.

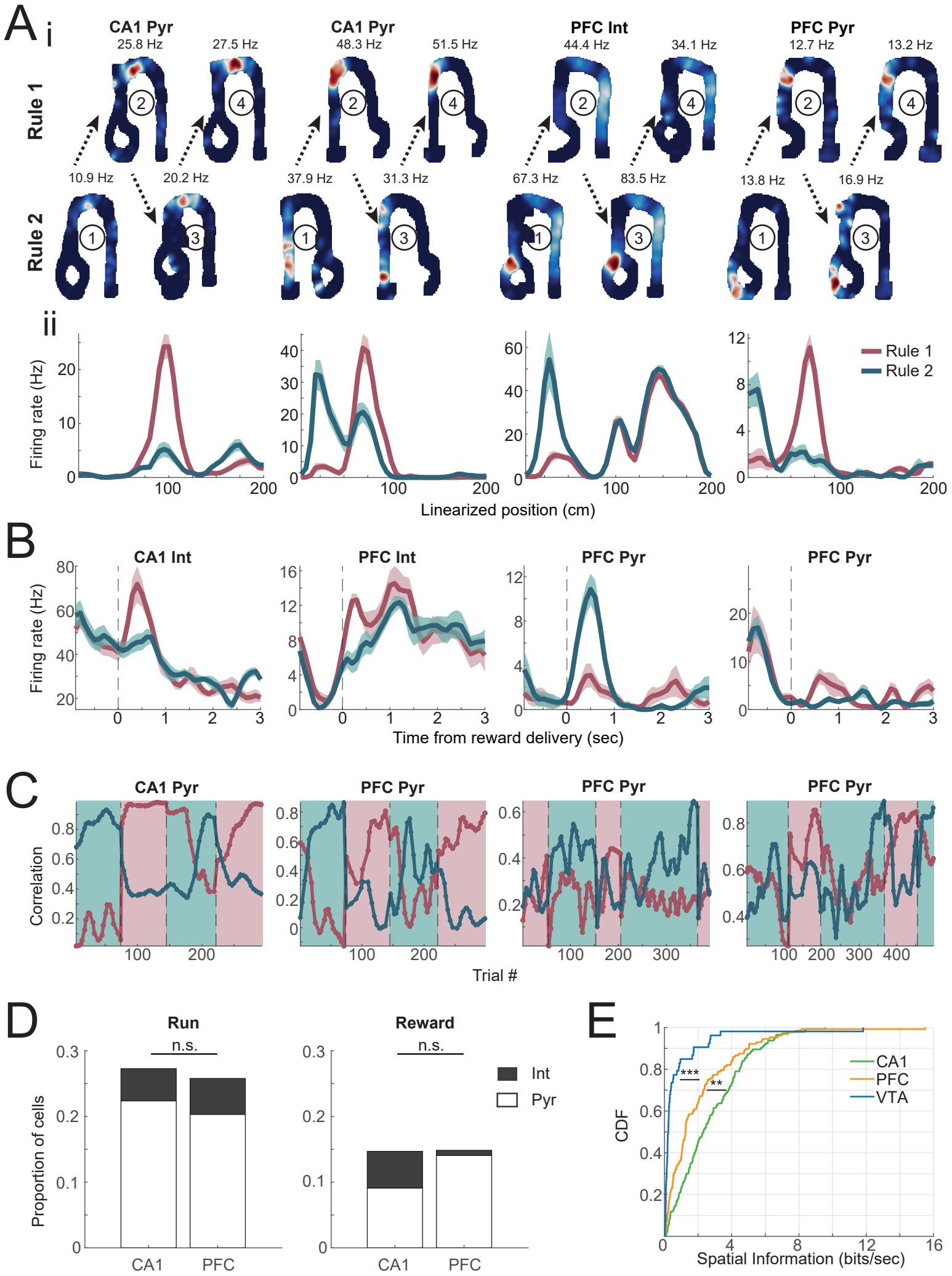
A
i
CA1 Pyr
25.8 Hz
27.5 Hz
CA1 Pyr
48.3 Hz
51.5 Hz
PFC Int
44.4 Hz
34.1 Hz
PFC Pyr
12.7 Hz
13.2 Hz
Rule 1
Rule 2
10.9 Hz
20.2 Hz
37.9 Hz
31.3 Hz
67.3 Hz
83.5 Hz
13.8 Hz
16.9 Hz
ii
Firing rate (Hz)
Rule 1
Rule 2
Linearized position (cm)
B
CA1 Int
PFC Int
PFC Pyr
PFC Pyr
Firing rate (Hz)
Time from reward delivery (sec)
C
CA1 Pyr
PFC Pyr
PFC Pyr
PFC Pyr
Correlation
Trial #
D
Run
n.s.
Reward
n.s.
Int
Pyr
Proportion of cells
CA1
PFC
E
CDF
CA1
PFC
VTA
***
**
Spatial Information (bits/sec)

Fig 2: Remapping of single cells in CA1 and PFC across rules.

A. Illustrative examples of spatial representations in CA1 and PFC showing remapping on the common trajectories performed across the two rules, Left-to-Center or Center-to-Left. (i). 2D place field at stable performance of rule 1 (*top*) and rule 2 (*bottom*) in interleaved blocks (first block for each rule showed on Left and second block shown on Right, numbers in circles denote order of blocks), with peak firing rate on top. Numbers in circles denote sequence of rule block; (ii). linearized firing fields of the cells shown above (mean ± standard error).

B. Illustrative examples showing firing rate change of neurons at the same well locations across the two rules, aligned to reward onset for the same common trajectory across rules (Left-to-Center or Center-to-Left).

C. Correlation of single cell firing patterns during individual trials to average firing patterns during stable performance of a given rule (> 60th percentile of the performance of the day) during rule switching blocks. Note the change in correlations that occur after rule switch.

D. Proportion of remapped cells for each region. During running: CA1 27.3% (39/143, 32 Pyr, 7 Int), PFC 25.8% (33/128, 26 Pyr, 7 Int), χ^2=0.077, p=0.78; At reward location: CA1 14.7% (21/143, 13 Pyr, 8 Int), PFC 14.8% (19/128, 18 Pyr, 1 Int), χ^2=0.0013, p=0.97, Fisher's exact test for proportions of remapped cells between regions.

E. Distribution of spatial information encoded by individual cells for each brain region. CA1: median 2.3 bits/sec, n=143; PFC: median 1.3 bits/sec, n=128; VTA: median 0.23 bits/sec, n=53. CA1-PFC p=0.0010, PFC-VTA p=6.2×10^{-8}, CA1-VTA p=7.7×10^{-17}, Kruskal-Wallis test with multi-comparison correction.

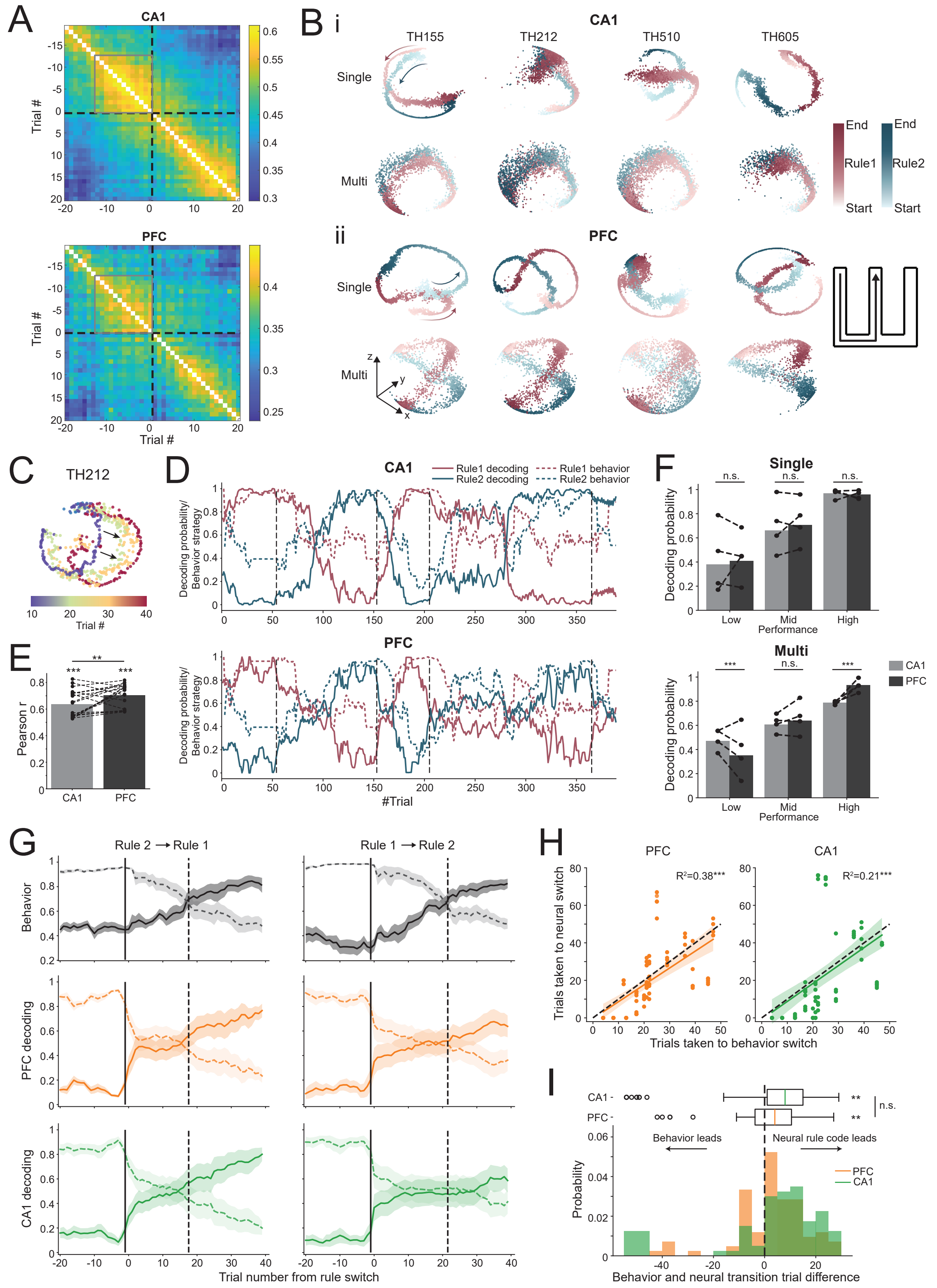
A
CA1
PFC
Trial #
B
i
ii
CA1
PFC
TH155
TH212
TH510
TH605
Single
Multi
End
Rule1
Start
End
Rule2
Start
C
TH212
Trial #
D
CA1
PFC
Rule1 decoding
Rule2 decoding
Rule1 behavior
Rule2 behavior
Decoding probability/
Behavior strategy
#Trial
E
Pearson r
CA1
PFC
F
Single
Multi
Decoding probability
Low
Mid
High
Performance
n.s.
CA1
PFC
G
Rule 2 → Rule 1
Rule 1 → Rule 2
Behavior
PFC decoding
CA1 decoding
Trial number from rule switch
H
PFC
CA1
R²=0.38***
R²=0.21***
Trials taken to neural switch
Trials taken to behavior switch
I
CA1
PFC
Behavior leads
Neural rule code leads
Probability
Behavior and neural transition trial difference

858 **Fig 3: PFC and CA1 ensembles encode rule representations and transitions**

859 A. Correlation of population activity vectors aligned to rule switch (dashed black line) in a
860 trial wise manner for CA1 and PFC. Note the weakened stability shown by lower
861 correlations following rule switches in both regions. Areas of stable correlations are
862 denoted by grey squares.

863 B. CA1 and PFC population activity show differential representation of the same trajectory
864 across rules. Populations activity space shown by dimensionality reduction using
865 CEBRA (see **Methods**). A particular 3D view is illustrated, with arbitrary units for axes. (i)
866 CA1 embeddings of the example common trajectory across rules (Left to Center,
867 schematic on bottom right). *Top*: 3D embedding from models trained using individual
868 animal's data; bottom: model trained with multi-session CEBRA with data from multiple
869 animals to capture common underlying structure across animals. Start and End denote
870 beginning and end of the same trajectory across the two rules. (ii) Embeddings of the
871 same trajectory but for PFC.

872 C. An illustrative example showing that the PFC population representation of the common
873 trajectory shifts in the manifold space (shift denoted by arrow) during rule transition over
874 the course of trials. Trajectory representations are grouped in 10 trials per color.

875 D. Decoding probability of each rule from an example animal shows CA1 (*top*) and PFC
876 (*bottom*) neural activity transitions from representing one rule to the other (Rule 1 in dark
877 red, Rule 2 in teal) over a few to tens of trials after each rule switching (rule switching is
878 denoted by dashed black vertical lines). Dashed colored curves show estimated
879 behavior strategy similarity to the optimized behavior for each rule.

880 E. CA1 and PFC rule decoding probabilities are highly correlated with behavior strategy.
881 Mean Pearson r: between CA1 and behavior 0.64±0.02, between PFC and behavior
882 0.70±0.02. Dots and dashed lines show correlation between behavior and each
883 decoding estimate (n=20, 4 animals, 5 estimates each, see **Methods**). p values for all

behavior-rule decoding correlations are less than 0.001. Behavior correlation with PFC rule decoding probabilities was higher than with CA1 decoding (p=0.0047, paired t test).

F. Rule decoding accuracy (proportion of trials decoded correctly) in each region, grouped by behavioral performance. *Top*: decoding accuracy of single-animal models (low performance: CA1, 0.38, PFC, 0.41, p=0.33 for CA1 vs PFC; mid performance: CA1, 0.66, PFC, 0.71, p=0.12; high performance: CA1, 0.97, PFC, 0.96, p=0.31, two-proportion z-test). *Bottom*: decoding accuracy using multi-animal models (low performance: CA1, 0.47, PFC, 0.35, $p=1.3\times10^{-4}$; mid performance: CA1, 0.61, PFC, 0.64, p=0.27; high performance: CA1, 0.79, PFC, 0.93, $p=9.9\times10^{-12}$). Dots and dashed lines show decoding accuracy for each animal under each condition (n=4 animals).

G. Behavior strategy similarity (top), probabilities of PFC rule decoding (middle) and CA1 rule decoding (bottom) aligned to rule switching trials, shown separately as Rule 2 to Rule 1 (left) and Rule 1 to Rule 2 (right) switches. On average, behavior transitions happened 17 (IQR: 13-29) trials after the Rule1 -> Rule2 switch, with PFC and CA1 neural representations slightly leading behavior. For the switch type of Rule 2 -> Rule 1, behavior started to reflect the new rule after 22 (IQR: 20.75-28.5) trials, with PFC leading in contrast to CA1 lagging.

H. Correlation between the number of trials taken for behavior switch and neural representation switch, combined across rule switch types. Dashed lines indicate diagonal lines where the timing of neural transitions equals that of behavior switches. Left: PFC and behavior, $R^2=0.38$, $p=3.4\times10^{-10}$; right: CA1 and behavior, $R^2=0.21$, $p=1.9\times10^{-5}$.

I. Distribution of timing differences between behavior switch and neural representation switch. Behavior relative to PFC transitions: median +4.0 (IQR: -3.75-10.5) trials, n=80, p=0.0044; behavior relative to CA1 transitions: median +8.0 (IQR: 1-15) trials, n=78,

909 p=0.0040, Wilcoxon signed rank test. For box plots, boxes, whiskers and circles indicate

910 quartile, 1.5×IQR and outliers, respectively.

911

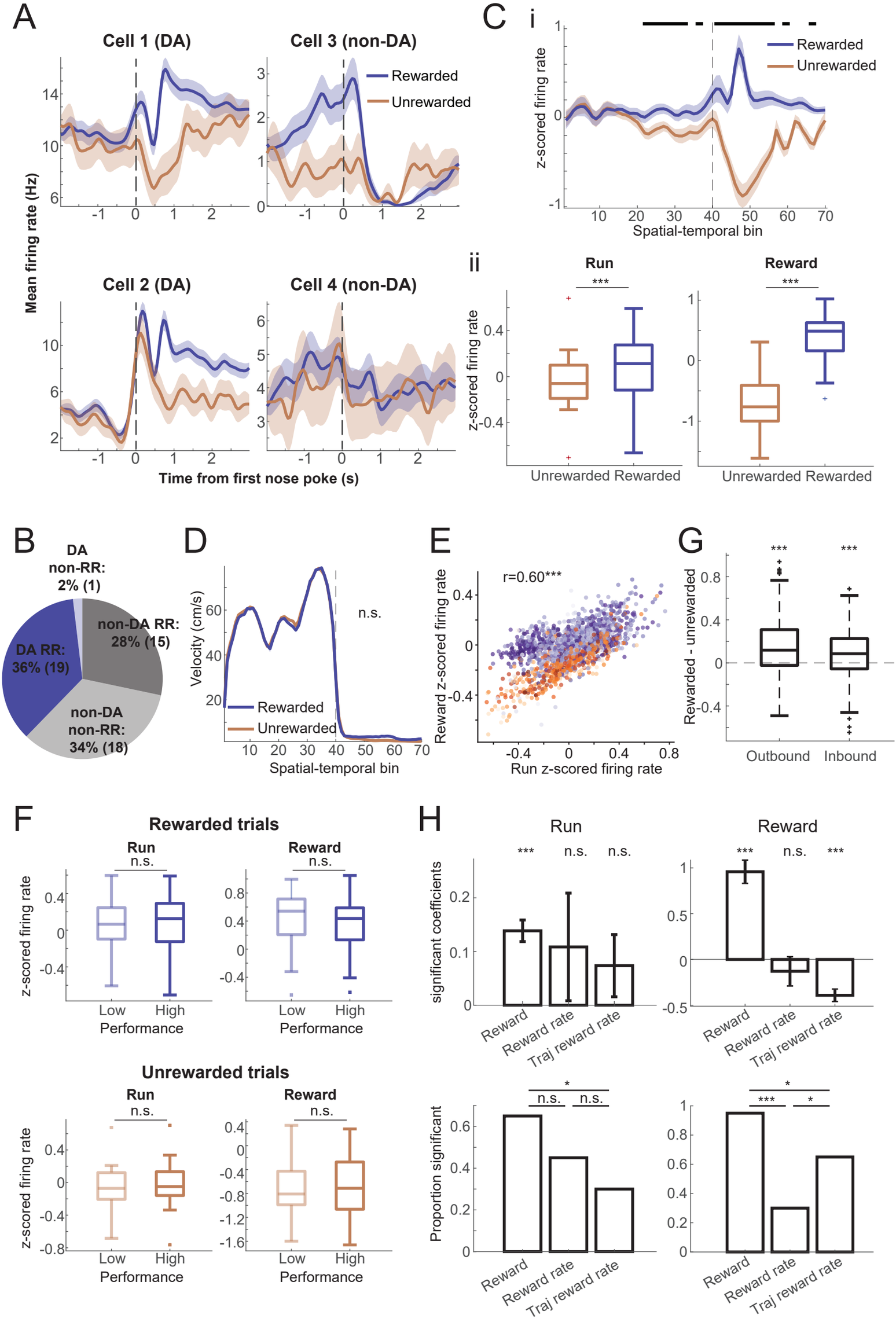
A
Cell 1 (DA)
Cell 3 (non-DA)
Cell 2 (DA)
Cell 4 (non-DA)
Rewarded
Unrewarded
Mean firing rate (Hz)
Time from first nose poke (s)
C
i
z-scored firing rate
Spatial-temporal bin
ii
Run
Reward
***
Unrewarded Rewarded
B
DA non-RR: 2% (1)
non-DA RR: 28% (15)
DA RR: 36% (19)
non-DA non-RR: 34% (18)
D
Velocity (cm/s)
n.s.
Rewarded
Unrewarded
Spatial-temporal bin
E
r=0.60***
Reward z-scored firing rate
Run z-scored firing rate
G
Rewarded - unrewarded
Outbound
Inbound
F
Rewarded trials
Unrewarded trials
Run
Reward
n.s.
z-scored firing rate
Low
High
Performance
H
Run
Reward
significant coefficients
Proportion significant
Reward
Reward rate
Traj reward rate

Fig 4: DA spiking activity mirrors reward prediction error.

A. Illustrative examples showing that DA neuronal firing activity at reward wells signals robust differences between rewarded and unrewarded outcomes. Left: example photo-tagged TH+ neurons; right: example non-DA neurons. Line: trial-averaged firing rate; shaded area: standard error.

B. Percentage of cell types and reward responses in VTA. RR: reward responsive at 200-1200ms after first nose pokes. DA RR 36% (19/53), DA non-RR 2% (1/53), non-DA RR 28% (15/53), non-DA non-RR 34% (18/53).

C. (i) Population response of putative DA neurons to reward outcomes during reward approach and at reward well. Bar on top indicates spatial/temporal bins with $p<0.05$ after Bonferroni correction using paired rank tests. Vertical black dotted line is first nose poke/ reward at the reward well, also corresponding to transition from spatial to temporal bins. Spatial bins during approach to reward well are from 1-40 (5-6 cm per bin, 200-240 cm in total), and temporal bins after arrival at reward well are from 41-70 (100 ms per bin, 3 seconds in total). (ii) average z-scored firing rates of all putative DA cells during rewarded vs unrewarded trials. Left: during run, starting from leaving the last reward/nose poke to the beginning of the current trial's reward/nose poke, rewarded median=0.11, unrewarded median = -0.060, $p = 1.8\times10^{-4}$; right: reward time (200ms-1200ms after the first nose poke), rewarded median=0.49, unrewarded median = -0.76, $p = 5.6\times10^{-5}$. Wilcoxon signed-rank test, n=20 cells.

D. Control for running speed during trial. No significant differences are seen in running speed between rewarded and unrewarded trials ($p = 0.12$).

E. Strong correlation of DA population firing rates during reward approach running and at reward outcome ($r = 0.60$, $p = 6.8\times10^{-148}$). Colors from light to dark indicate performance from low to high. Red: error trials; blue: correct trials.

F. DA firing rates show no difference between low- and high-performance period. Top: rewarded trials (median z-scored firing rate during running: low performance 0.065, high performance 0.13, p=0.23; during reward outcome: low performance 0.54, high performance 0.44, p=1.00); bottom: unrewarded trials. (run: low performance -0.072, high performance -0.049, p=0.23; outcome: low performance -0.81, high performance -0.71, p=0.65, Wilcoxon paired rank test, n=20 cells).

G. Difference in DA firing rates for rewarded vs unrewarded trials during running is present for both inbound trials (median difference 0.085, $p = 1.8\times10^{-6}$, n = 178 trials) and outbound trials (median difference 0.12, $p = 1.0\times10^{-13}$, n = 217 trials).

H. Multiple regression for DA neuron firing rates during run or reward outcome using the following parameters: current-trial reward, reward rate of the last 5 trials, reward rate the same trajectory for the last 5 visits. *Top*: mean significant coefficients. Current-trial reward: run: $\beta = 0.14\pm0.02$ (mean±sem), $p=2.4\times10^{-4}$; outcome: $\beta = 0.95\pm0.13$, $p=1.6\times10^{-4}$; reward rate: run: $\beta = 0.11\pm0.10$, p=0.36; outcome: $\beta = -0.13\pm0.16$, p=0.56; same-trajectory reward rate: run: $\beta = 0.074\pm0.058$, p=0.16; outcome: $\beta = -0.39\pm0.07$, $p=2.4\times10^{-4}$, Wilcoxon signed rank test. *Bottom*: Proportions of DA neurons modulated by each factor. Run: current reward 65% vs reward rate 45%: $\chi^2=1.6$, p=0.20; current reward 65% vs same-trajectory reward rate 30%: $\chi^2=4.9$, p=0.027; reward rate 45% vs same-trajectory reward rate 30%: $\chi^2=0.96$, p=0.33. Outcome: current reward 95% vs reward rate 30%: $\chi^2=18.0$, $p=2.2\times10^{-5}$; current reward 95% vs same-trajectory reward rate 65%: $\chi^2=5.6$, p=0.018; reward rate 30% vs same-trajectory reward rate 65%: $\chi^2=4.9$, p=0.027. Fisher's exact test, n=20 cells.

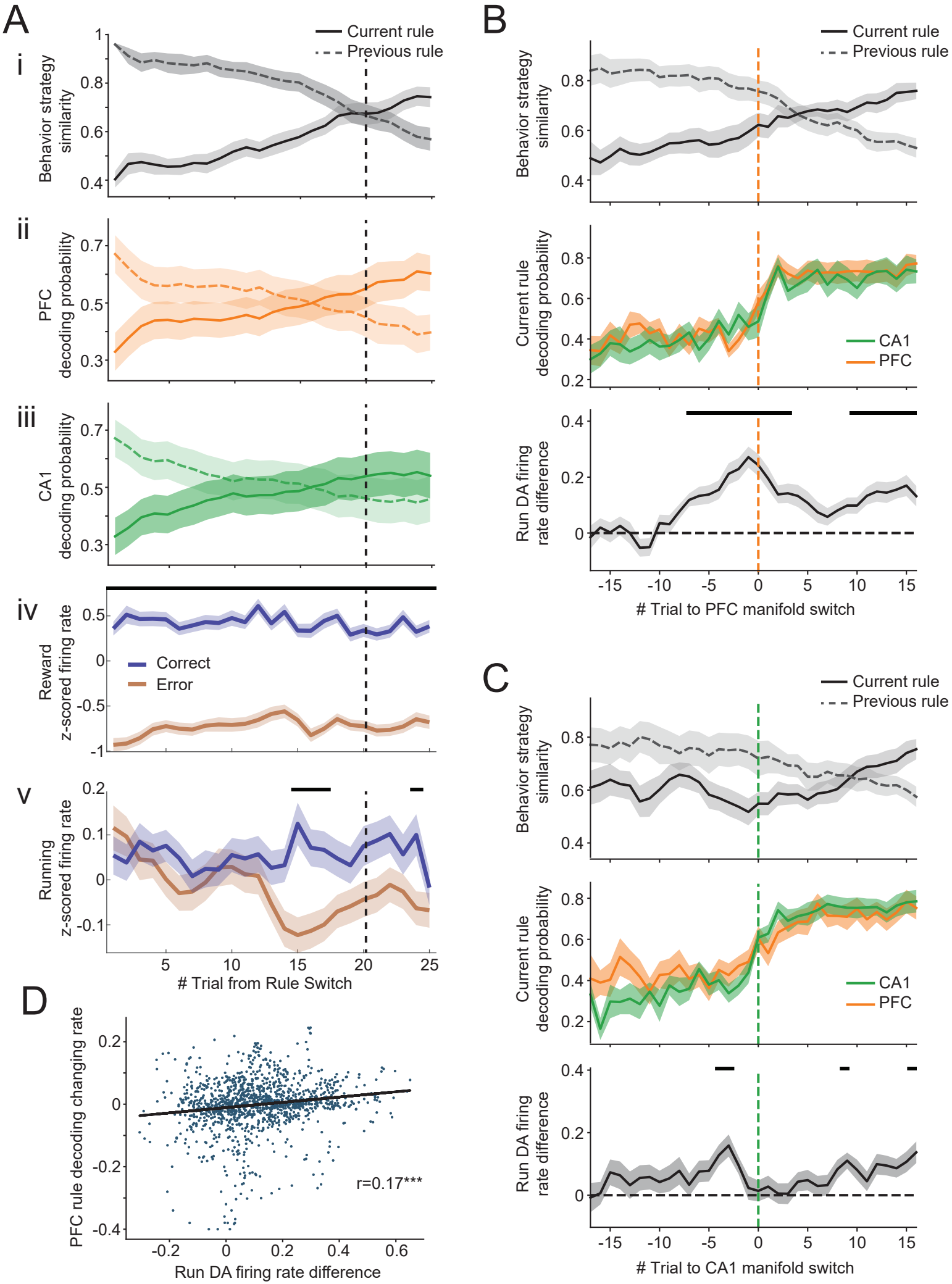
A
i
Current rule
Previous rule
Behavior strategy similarity
ii
PFC decoding probability
iii
CA1 decoding probability
iv
Reward z-scored firing rate
Correct
Error
v
Running z-scored firing rate
Trial from Rule Switch
B
Behavior strategy similarity
Current rule decoding probability
CA1
PFC
Run DA firing rate difference
Trial to PFC manifold switch
C
Behavior strategy similarity
Current rule decoding probability
CA1
PFC
Run DA firing rate difference
Trial to CA1 manifold switch
D
PFC rule decoding changing rate
r=0.17***
Run DA firing rate difference

Fig 5: DA spiking activity relationship with neural manifold change and rule switching behavior.

A. Behavior strategy (i), PFC (ii) and CA1 (iii) decoding probability changes aligned to rule switching trials. (iv-v). Difference in DA neuron firing rates for rewarded vs unrewarded trials at well locations (iv) and during running (v), plotted as a function of trials aligned to beginning of rule switch. Black bars indicate significant difference between rewarded and unrewarded trials with $p<0.05$ after Bonferroni correction. Vertical black dotted line across sub-panels denotes behavioral strategy switch trial.

B. Behavior strategy, CA1/PFC decoding probability changes and DA firing rate differences between rewarded and unrewarded trials, aligned to decoded rule representation switch in PFC (vertical orange dotted line). Top: Behavior strategy similarity to optimized behavior of current and previous rules. Animals' behavior adapted to the new rule on average 4 (IQR: -3.75-10.5) trials after PFC showed correct rule decoding. Middle: CA1 and PFC decoding accuracy of current rule. Bottom: DA firing rate difference for rewarded vs unrewarded trials during running. Black bars above indicate trials showing significant difference with $p<0.05$ after Bonferroni correction.

C. Same as B but aligned to CA1 rule representation switch (vertical green dotted line).

D. DA firing activity difference between rewarded and unrewarded trials is correlated with changing rate of PFC manifold (Pearson correlation $r = 0.16$, $p = 2.8\times10^{-9}$, $n=1361$ trials).